Circ J 2008; **72:** 1615 – 1620

Anatomical Investigation of the Sinus Node Artery Using Dual-Source Computed Tomography

Long Jiang Zhang, MD; Yu Zhu Wang, Bachelor; Wei Huang, MD;
Peng Chen, MS; Chang Sheng Zhou, Bachelor; Guang Ming Lu, MD

Background Few investigators have studied the anatomy of the sinus node artery (SNA) using noninvasive imaging modalities, so the objective of this study was to visualize the in-vivo 3-dimensional anatomical relations of the SNA using dual-source computed tomography (DSCT).

Methods and Results In the 101 patients included in this study, the visualization rate, anatomical type and diameter of the SNA, the distance between the orifice and coronary artery, and the terminal type of SNA were recorded. The visualization rate was 95.2% (96/101). Of 96 patients, 106 SNAs were detected among which 51 (48.1%, 51/106) originated from the right coronary artery, 52 (49.1%, 52/106) from the left circumflex artery, and 3 (2.7%, 3/106) from other branches. There were 3 types of SNA: right (n=52), left (n=45), and posterior (n=9). The distance between the orifice of the right SNA and the right coronary sinus was 14.2±15.2 mm, for the left SNA it was 5.5±3.5 mm, and for the posterior SNA, 33.7±12.8 mm. The average diameter was 1.27±0.29 mm. The SNA approached the nodal tissue by 1 of 3 routes: retrocaval (51.5%), precaval (25.2%), or pericaval (22.3%).

Conclusion The SNA can be visualized in vivo using DSCT, which is important for preoperative knowledge of its origin, course, termination, and anatomical type. (*Circ J* 2008; **72:** 1615 – 1620)

Key Words: Computed tomography; Coronary artery disease; Sinus node artery; X-ray

The sinuatrial nodal artery (SNA), which is the sinuatrial nodal branch of the coronary arteries, is anatomically significant because it is a landmark for the identification of the sinoatrial node (SAN), in addition to its own clinical significance[1,2] According to previous reports, the SNA has only 1 branch in 90–100% of hearts;[3–10] which shows that compensation cannot occur in the case of it being cut off or occluded[7] In addition, its close relationship with the atrium can result in injury during atrial surgery[3] Therefore, it is very important to assess in vivo the origin, course, route, and distribution of the SNA. Computed tomography (CT) has been used to visualize the in vivo anatomy of coronary arteries;[11–14] but only a few investigators have studied the anatomy of the SNA using electron-beam CT (EBCT) or 64-slice CT;[11,12] either of which has difficulty in delineating the detailed anatomy of the SNA because of their limited spatial and/or temporal resolution. Dual-source CT (DSCT), with its double array consisting of an X-ray tube and detectors arranged at a 90-degree angles to each other, and a gantry rotation time of 330 ms, allows for a temporal resolution of 83 ms at the center of gantry rotation when half-scan image reconstruction algorithms are used[15–19] This temporal resolution makes it feasible to use DSCT as a useful screening modality for detecting coronary artery disease[16,20–24] To the best of our knowledge, there are few studies of the in vivo visualization of the SNA using noninvasive imaging modalities[11,12] and so our purpose was to assess the anatomical types of SNA using DSCT.

(Received March 4, 2008; revised manuscript received May 1, 2008; accepted May 13, 2008; released online August 27, 2008)
Department of Medical Imaging, Jinling Hospital, Clinical School of Medical College, Nanjing University, Nangjing, Jiangsu Province, China
Mailing address: Guang Ming Lu, Department of Medical Imaging, Jinling Hospital, Clinical School of Medical College, Nanjing University, Zhongshan East Road 305, Xuanwu District, Nanjing, Jiangsu Province 200012, China

Methods

Study Population

Between July 2007 and August 2007, 101 patients (67 males, 34 females; age range 35–87 years, average age 59±13 years) suspected of having coronary artery disease or valve disease underwent DSCT coronary angiography (CAG). Exclusion criteria for DSCT were allergy to iodine-containing contrast medium, renal insufficiency (creatinine level >120 mol/L), pregnancy, any heart rhythm other than sinus rhythm, hemodynamic instability, respiration motion artifact, and previous bypass surgery.

Patient Preparation

All subjects gave written informed consent before the examination. Irrespective of the individual's heart rate or variability, β-blockers were not administered prior to the scan. All subjects inhaled nitroglycerin (0.1 mg; Nitroglycerin Inhaler Shandong Jingwei Pharmacy Ltd Corp, Ji'nan, China) to dilate the coronary arteries 5 min prior to DSCT CAG. All subjects were in sinus rhythm throughout the scan.

Scan Protocol and Image Reconstruction

All CT examinations were performed using a DSCT scanner (Somatom Definition, Siemens AG, Medical Solutions, Forchheim, Germany). The patients were centrally placed in the scanner to ensure that the entire heart was covered with

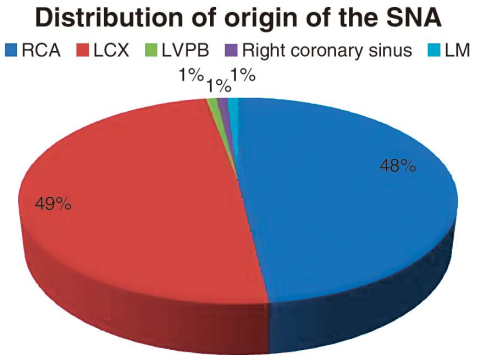

Fig 1. Distribution of the origin of the SNA. SNA, sinus node artery; RCA, right coronary artery; LCX, left circumflex artery; LVPB, left ventricular posterior branch; LM, left main stem.

the smaller field-of-view of the second tube detector array. CAG scanning was started by continuously injecting a bolus of 80 ml of Ultravist (370 mg I/ml, Schering, Germany), followed by 40 ml saline solution, into an antecubital vein via an 18-gauge catheter (injection rate 5 ml/s). Contrast agent application was controlled by bolus tracking technique. A region of interest was placed at the aortic root, and image acquisition started 5 s after the signal attenuation reached the predefined threshold of 100 Hounsfield units. ECG pulsing for radiation dose reduction was used for all patients. At a mean heart rate <60 beats/min, the full tube current was applied from 60 to 70%, at 61–70 beats/min from 50 to 80%, and at heart rates >70 beats/min from 30 to 80% of the R-R interval. The average heart rate during scanning was 76.93±14.83 beats/min. A retrospective gating technique was used to synchronize the data reconstruction with the ECG signal. A monosegment reconstruction algorithm that uses the data from a quarter rotation of both de-

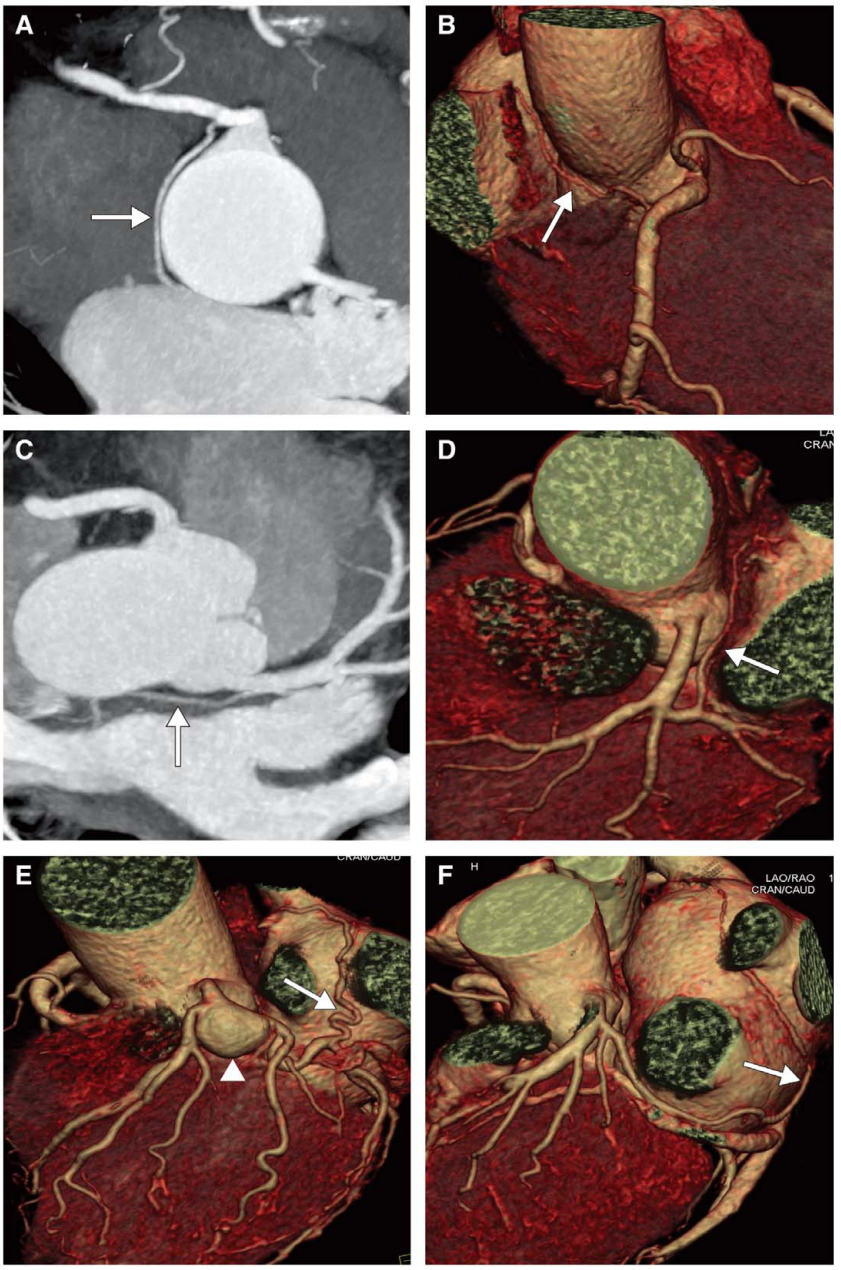

Fig 2. Types of SNA. Right SNA: MIP (A) and VR (B) images show the right SNA from the proximal segment of the RCA, coursing towards the artifice of the SVC (arrow). Left SNA: thin-slab MIP (C) and VR (D) images show the left SNA from the proximal segment of LCX, coursing towards the artifice of the SVC (arrow). (E) Left posterior SNA: VR image shows the left posterior SNA from the LCX, coursing between the left artrial appendage and left superior pulmonary vein towards the SVC (arrow). Note the aneurysm at the bifurcation of the LM (arrowhead). (F) Left posterior SNA: VR image shows the left posterior SNA directly originating from the LCX, coursing between the artrial appendage and left superior pulmonary vein towards the SVC (arrow). MIP, maximum intensity projection; SVC, superior vena cava; VR, volume rendered. Other abbreviations see Fig 1.

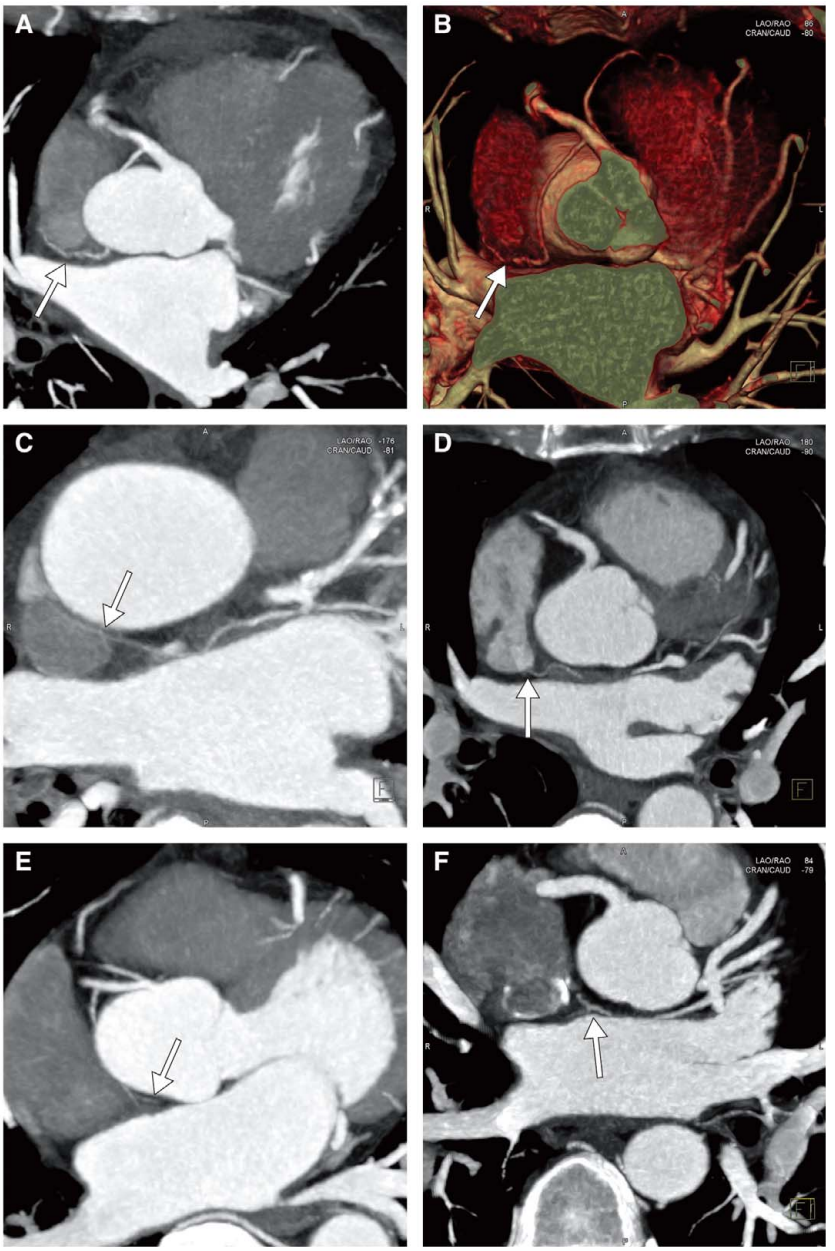

Fig 3. Types of terminal SNA related to the SVC. (A, B) Right retrovacal SNA shown in the oblique MIP and VR images. The SNA arises from the proximal segment of RCA, courses posterior between the SVC and the root of aorta, terminating at the posterior side of the SVC (arrow). (C) Left prevacal SNA in a MIP image. The SNA arises from the proximal segment of LCX, courses right between the left atrium and the root of the aorta, terminating at the anterior aspect of the SVC (arrow). (D) Left retrovacal SNA in an oblique MIP image. The SNA arises from the proximal segment of LCX, courses right between the left atrium and the root of the aorta, terminating at the posterior aspect of the SVC (arrow). (E) Right perivacal SNA in a MIP image. The SNA arises from the proximal segment of the RCA, courses posteriorly between the SVC and the root of the aorta, surrounding the orifice of the SVC (arrow). (F) Left perivacal SNA in a MIP image. The SNA arises from the proximal segment of the LCX, courses right between the left atrium and the root of aorta, surrounding the orifice of the SVC (arrow). See Figs 1 and 2 for abbreviations.

tectors was used for image reconstruction. In each patient, images were first previewed in 5% steps to select the optimal phase for post-processing. If considered necessary (ie, poor image quality), additional images were reconstructed in 5% steps from 20 to 80% of the R-R interval, then a 4-dimensional tool was used to select the optimal reconstruction phase. For CAG, images were reconstructed from the contrast-enhanced DSCT scan with a slice thickness of 0.75 mm, a reconstruction increment of 0.5 mm, and using a medium soft-tissue convolution kernel (B26f). Depending on the individual anatomy, the reconstructed field-of-view was adjusted to encompass the heart exactly (image matrix 512×512 pixels).

Image Analysis

After removing each patient's personal information, reconstructed images were transferred to a dedicated workstation (Wizard, Siemens AG, Medical Solutions) equipped with dedicated cardiac post-processing software (Syngo Circulation, Siemens AG, Medical Solutions). Multiplanar reformation, maximum intensity projection, and volume rendering (VR) were performed by an experienced radiologist (Zhang LJ). VR images were reconstructed to analyze the course of the SNA and its relationship with adjacent structures. Various reformations of the transverse images were rendered and evaluated in consensus by 2 radiologists (Z.L.J. and W.Y.Z. with 6 and 2 years of experience in CT interpretation, respectively).

Coronary vessels were studied to find the dominant vessel. The origin, number, and course of the SNA were analyzed to determine the anatomical type of SNA on the thin section. Next, the diameter of the SNA and the distance between it and the orifice of its relevant coronary artery were measured on the axial section or the reconstructed images. For the SNA from the right coronary artery (RCA), the distance between its origin and the right coronary sinus

Table 1 Morphological Types of Terminal Segment of SNA

Type	*Right SNA*	*Left SNA*	*Posterior SNA*	*Overall*
Branches	*52 (49.1%)*	*45 (42.5%)*	*9 (8.4%)*	*106 (100%)*
Branches shown	*52 (100%)*	*43 (95.6%)*	*8 (88.9%)*	*103 (97.2%)*
Type of terminal SNA				
Pericaval (n)	*10 (19.2%)*	*13 (30.2%)*	*0 (0%)*	*23 (22.3%)*
Precaval (n)	*8 (15.4%)*	*16 (37.2%)*	*3 (37.5%)*	*27 (26.2%)*
Retrocaval (n)	*34 (65.4%)*	*14 (32.6%)*	*5 (62.5%)*	*53 (51.5%)*

SNA, sinuatrial nodal artery.

Table 2 Diameter of SNA and Distance Between Its Origin and Relevant Coronary Orifice

Index	*All SNA*	*Right SNA*	*Left SNA*	*Posterior SNA*
Mean diameter (mm, range)	*1.27±0.3 (0.48–2.11)*	*1.3±0.3 (0.9–1.8)*	*1.3±0.4 (0.5–2.1)*	*1.2±0.2 (0.9–1.5)*
Diameter of SNA				
<1 mm (n)	*15 (14%)*	*5 (10%)*	*8 (18%)*	*2 (22%)*
1.0–1.5 mm (n)	*71 (67%)*	*37 (71%)*	*27 (60%)*	*7 (78%)*
>1.5 mm (n)	*20 (19%)*	*10 (19%)*	*10 (22%)*	*0 (0%)*
Mean distance (mm, range)	*14.2±15.2 (0–120.3)*	*16.4±9.5 (0–38.9)*	*5.5±3.5 (1.4–14.5)*	*33.7±12.8 (8.8–120.3)*
Distance to coronary orifice				
≤10 mm (n)	*58 (54%)*	*18 (35%)*	*39 (87%)*	*1 (11%)*
11–20 mm (n)	*24 (23%)*	*18 (35%)*	*6 (13%)*	*0 (0%)*
>20 mm (n)	*24 (23%)*	*16 (30%)*	*0 (0%)*	*8 (89%)*

SNA, sinuatrial nodal artery.

was measured, whereas for the SNA from the left coronary arteries, including the left main stem (LM) and left circumflex artery (LCX), the distance between the origin of the SNA to the orifice of the LCX (or LM) was measured. The diameter of the SNA and the distance to its relevant coronary artery orifice were summarized and classified for all cases. The mode of termination of the SNA in relation to the superior vena cava (SVC) was classified as retrocaval, precaval, or pericaval. The walls of the SNA and of the coronary segment 2 cm proximal to the SNA were assessed for the presence of calcified and noncalcified atherosclerotic plaque.

Results

Of 101 patients, the origin, course, and termination of SNA were clearly shown in 96 (65 males, 31 females; mean age 59±13 years); 5 patients were excluded because of difficulty in recognizing the SNA (not detected, n=4; poor image quality, n=1). Therefore, in this study the incidence of visualizing the SNA was 95.2% (96/101). In the 96 patients there were 106 branches of the SNA (Figs 1,2): a single SNA in 86 patients and dual SNAs in 10 patients. Of the 86 subjects with a single SNA, 44 arose from the RCA (51%) and in the other 42 subjects it was from the LCX (49%), including 8 SNAs from the posterolateral LCX. All the dual SNAs originated from the RCA and the LCX. The terminal segments of 103 SNA relative to the SVC were shown by DSCT; of these, the SNA approached the SAN anterior to the SVC (precaval) in 26 (26.2%) branches, posterior to the SVC (retrocaval) in 53 (51.5%) branches, and through multiple branches surrounding the SVC (pericaval) in 23 (22.3%) branches (Fig 3).

We grouped the SNA into 3 types and 9 subtypes (Table 1) according to the origin, course, and termination.

(1) Right SNA (49.1%, 52/106) (Figs 2A,B) originating from the RCA (n=51) or right coronary sinus (n=1), and coursing between the right atrium and the root of aorta toward the ostium of the SVC.

(2) Left SNA (42.5%, 45/106, Figs 2C,D) originating from the proximal segment of the LCX and coursing along the anterior wall of the left atrium, terminating at the ostium of the SVC.

(3) Posterior SNA (8.4%, 9/106) originating from the posterolateral segment of the LCX (n=7, Fig 2E), LM (n=1, Fig 2F), or left ventricular posterior branch of the RCA (n=1). This type of SNA always followed the same route, coursing backward in a groove at the junction the mouth of the left atrial appendage and the orifice of the left superior pulmonary vein (Fig 2E). In this groove, the artery was in close proximity to the left superior pulmonary vein ostium and it then followed the course observed for other left SNAs, traveling along the transverse sinus toward the SVC.

The diameter and distance between the origin of the SNA and its relevant orifice for the different types are shown in Table 2. The diameter of most SNAs ranged from 1.0 mm to 1.5 mm; the distance between the RCA ostium and the origin of the SNA did not have a dominant length, whereas the distance between the LCX ostium and the origin of the left SNA was less than 10 mm in most cases (87% of all left SNAs). The distance between the LCX ostium and the origin of a posterior SNA was longer than that of a left SNA, 89% of which originated more than 20 mm distal to the orifice of the LCX.

In 8 patients there were calcified (n=6) or noncalcified (n=2) plaques within the 2 cm proximal to the orifice of the SNA, and were in the RCA (n=4) and LCX (n=4), respectively. No significant stenosis (≥50%) was found in any of the 8 cases.

Discussion

Anatomical descriptions of the blood supply of the SNA have been reported previously;[3–10] but have been based solely on detailed cadaveric dissections and/or angiographic studies. However, it is difficult to dissect the SNA because

of its tortuous course within the heart and although conventional CAG is the gold standard for clearly delineating the anatomical origin, course, and distribution of the SNA, it is an invasive technique associated with some complications and risks. A few studies describing the anatomic origin and course of SNA using noninvasive imaging modalities have been reported[11,12] Stratznig et al showed that the incidence of visualizing the SNA was only 75% (60/80) because of poor image quality and the low spatial resolution of the EBCT scanner[11] Saremi et al recently studied the in vivo anatomy of the SNA using 64-slice CT and the SNA was not visualized in only 1 patient of their study group[12] DSCT, with its 2 arrays consisting of an X-ray tube and detectors arranged at a 90-degrees to each other and with a gantry rotation time of 330 ms, enables temporal resolution of 83 ms at the center of the gantry rotation when half-scan image reconstruction algorithms are used[15–19] The high temporal resolution, and the spatial resolution of 0.4 mm of DSCT, compared with the 165 ms of temporal resolution of 64-slice CT, improves the delineation of the smaller branches of the coronary arteries, such as the SNA. For ECG-gated CT CAG, image noise equivalent to that of multidetector row CT can be achieved with DSCT at doses comparable to or up to a factor of 2 lower than the doses used for multidetector row CT, depending on heart rate of the patient[25] In the present study, the rate of delineation of the SNA by DSCT was 95.2%, higher than that with EBCT. We also found that the anatomical origin and course of the SNA, and its relationship with adjacent structures, can be clearly assessed by DSCT, which is without doubt, very important for the preoperative planning of atrial surgery that involves the SAN.

This study showed that 106 branches of the SNA were visualized in 96 patients, with a single SNA observed in 86 patients and dual SNA in 10 patients; 48.1% of the SNA (51/106) arose from the RCA, while 42.5% arose from the proximal segment of the LCX, 6.6% (7/106) from the posterolateral part of the LCX, and 0.9% from the left ventricular posterior branch of the RCA (n=1), right coronary sinus (n=1) or LM (n=1). The anatomical findings in this study compare well with those reported by Yao et al who found that 48.7% of the SNAs originated from the RCA, 34.9% (53/150) from the proximal segment of the LCX, and 15.8% (24/150) from the posterolateral segment of LCX in a study of 150 Chinese human cadaveric hearts[3] However, our findings do not agree well with other studies in which the SNA predominantly originated from the RCA[4–10] Berdajs et al found that 66% of the SNAs originated from the RCA, and 34% from the LCX[4] Hadzeiselimovic et al found that 60% of the SNAs originated from the RCA and 40% from the LCX in 200 cadaveric hearts[5] and Bokeriya et al found 61.4% of the SNAs originated from the RCA and 38.4% from the LCX in 70 cadaveric hearts[6] Recently, Saremi et al[12] reported that a single SNA arose from the RCA in 67 (65.7%) cases and from the LCX in 28 (27.4%) cases; dual blood supply to the SAN was seen in 6 (5.9%) cases among the 102 hearts studied. From these descriptions, the origin dominance of the SNA in Chinese appears to differ from that for Western subjects. Approximate 50% of SNAs arise from the RCA and LCX in Chinese, whereas in Western studies the origin of the SNA is predominantly from the RCA. This may be a race difference, although a Japanese study of the gross anatomy of the SNA in 30 hearts showed that the SNA was supplied by the RCA more frequently (73% of cases) than by the left LCX (3%), and in 23% of cases the node was supplied by both coronary arteries[10]

We measured the diameter of the SNA and the distance between its origin and the relevant coronary orifice. The diameter of most SNAs ranged from 1.0 to 1.5 mm; the distance between the RCA ostium and the origin of the SNA did not have a dominant type, whereas the distance between the LCX ostium and the origin of the left SNA was less than 10 mm in most cases, accounting for 87% of all left SNAs. The distance between the LCX ostium and the origin of a posterior SNA was longer than that for a left SNA, 89% of which were longer than 20 mm. Our study results compare well with those from a recent study of the anatomy of the SNA using 64-slice CT in which Saremi et al found the distance between the RCA ostium and the origin of the right SNA ranged from 0 to 40 mm (mean, 16±7 mm) and the distance between the LCX artery ostium and the origin of the left SNA ranged from 2 to 35 mm (mean, 12±6 mm)[12]

Some classifications of the types of SNA have been advocated[3,4,7] Kawashima et al classified the SNA into 6 types: (1) right anterior, (2) right posterior, (3) right lateral, (4) left anterior, (5) left posterior, and (6) left lateral, depending on origin, course, and distribution[7] Type 1 is a branch originating from the proximal portion of the RCA, running by the ventral (anterior) aspect of the SVC, and supplying the SAN. Type 2 is a branch originating from the proximal portion of the RCA, running by the dorsal (posterior) aspect of the SVC, and supplying the SAN. Type 3 is a branch originating from the RCA more distally than the medial border of the right auricular appendage, running by the lateral aspect of the right atrium, and supplying the SAN. Type 4 is a branch originating from the proximal portion of the LCX, running by the ventral (anterior) aspect of the SVC, and supplying the SAN. Type 5 is a branch originating from the proximal portion of the LCX, running by the dorsal (posterior) aspect of the SVC, and supplying the SAN. Type 6 is a branch originating from the proximal portion of the LCX more distally than the medial border of the left auricular appendage, running by the lateral aspect of the left atrium, and supplying the SAN. In Berdajs et al's study of 50 hearts, they was divided the SNAs into 2 types; that is, right and left SNAs, with the right SNAs further classified into type 1 (branching proximal to the right marginal branch, including 3 subtypes: course on the right, left or both sides of the SVC) and type 2 (branching distal to the right marginal branch) according to the origin of the right SNA[4] Yao et al classified the SNA in 150 cadaveric hearts into 3 types; that is, right, left, and left posterior SNA[3] We classified the SNAs into 3 types (right, left and posterior) and 9 subtypes (precaval, retrocaval, and pericaval) according to the origin and termination of the SNA (Table 1). The posterior type of SNA (ie, an S-shaped SNA) was advocated as an individual type of SNA in that right posterior SNA was found in this study, and has been reported[26]

We found a variant of the left SNA with an S-shaped course arising from the posterolateral part of the LCX artery in 8 cases and from the RCA in 1 case. McAlpine provided a detailed description of the posterior SNA[27] and Nerantzis and Avgoustakis[28] described it as a long S-shaped artery originating in the posterolateral part of the LCX artery below or behind the left auricle. In their coronary artery study of 300 human hearts, this anatomy was observed in 21% of the cases in which the SNA arose from the LCX artery (8% of all the hearts). Saremi et al found that this S-shaped artery was present in 5.9% of all cases and 18%

of left SNA;[12] while we found the incidence of posterior SNA was 8.4% of all cases, which corresponded closely to the anatomic dissection data reported by Nerantzis and Avgoustakis:[28] A posterior SNA was larger than the normal SNA and supplied the SAN and surrounding area, almost the entire left atrium, and a large part of the interatrial septum and right atrium, as well as part of the atrioventricular area. The incidence of rhythm disturbance varies from 52% to 60% of cases after the superior transseptal approach and the risk of intraoperative damage to the SNA during the superior transseptal approach to the mitral valve is high; therefore, knowledge of such arterial anatomy before operation will ensure preservation of the SAN in the patient:[26,29]

Study Limitations

The anatomy discussed in our study requires a high degree of precision that is available in vivo only with CT angiography; thus, we had no standard of reference with which to compare our findings. However, the anatomic agreement of our findings with historical cadaveric dissections of the human heart underlines the validity of our observations. Though the high temporal resolution of DSCT scanners improves the visualization of the coronary arteries and smaller branches, it is rather difficult to clearly display the terminal segment of coronary arteries even with state-of-the-art DSCT scanners. Thus, in this study bias can occur for the subtypes of SNA. Comparison with invasive CAG needs to be performed to clarify the accuracy of detecting the SNA by DSCT. In addition, the small size of the study group and the predominance of structurally normal hearts in our cohort limit broad generalization of our findings, especially to pathologically altered states. Finally, all classification of the vessels was made by consensus of 2 reviewers, and we provide no analysis of the interobserver agreement on the anatomy of these vessels.

In conclusion, we found that the origin, course, distribution and termination of the SNA, and its relationship with adjacent structures can be clearly shown using DSCT, and our findings compared well with previously published data obtained from cadaveric dissection and angiographic studies. We believe in vivo visualization of the SNA using DSCT is feasible, and has clinical implications for certain catheter-based or surgical procedures that have a potential risk of injurying the SNA and thus reducing the incidence of atrial arrhythmias resulting from postoperative impairment of the SAN.

References

1. Ando G, Gaspardone A, Proietti I. Acute thrombosis of the sinus node artery: Arrhythmological implications. *Heart* 2003; **89:** e5.
2. Kyriakidis M, Barbetseas J, Antonopoulos A, Skouros C, Tentolouris C, Toutouzas P. Early atrial arrhythmias in acute myocardial infarction: Role of the sinus node artery. *Chest* 1992; **101:** 944–947.
3. Yao ZB, Ren GL. Clinical anatomy of sinus node artery. *Chin Clin Anat J* 1995; **13:** 171–173 (in Chinese).
4. Berdajs D, Patonay L, Turina MI. The clinical anatomy of the sinus node artery. *Ann Thorac Surg* 2003; **76:** 732–736.
5. Hadzeiselimovic H. Vascularization of the conducting system in the human heart. *Acta Anat* 1978; **102:** 105–110.
6. Bokeriva LA, Mikhailin SL, Revishvili AS. Anatomical variants of sinoatrial and atrioventricular node arteries. *Cor Vasa* 1984; **26:** 220–228.
7. Kawashima T, Sasaki H. The morphological significance of the human sinuatrial nodal branch (artery). *Heart Vessels* 2003; **18:** 213–219.
8. Kyriakidis M, Vyssoulis G, Barbetseas J, Toutouzas P. Clinical angiographic study of the arterial blood supply to the sinus node. *Chest* 1988; **94:** 1054–1057.
9. Ortale JR, Paganoti C de F, Marchiori GF. Anatomical variations in the human sinuatrial nodal artery. *Clinics* 2006; **61:** 551–558.
10. Futami C, Tanuma K, Tanuma Y, Saito T. The arterial blood supply of the conducting system in normal human hearts. *Surg Radiol Anat* 2003; **25:** 42–49.
11. Stratznig P, Groell R, Rienmueller R. Detection of the sinus node artery using electron beam computed tomography of the heart. *Int J Cardiovasc Imaging* 2002; **18:** 457–461.
12. Saremi F, Abolhoda A, Ashikyan O, Milliken JG, Narula J, Gurudevan SV, et al. Arterial supply to sinuatrial and atrioventricular nodes: Imaging with multidetector CT. *Radiology* 2007; **246:** 99–107.
13. Jinzaki M, Yamada M, Sato K, Tanami Y, Anzai T, Sasaki K, et al. Overview image of the lumen and vessel wall in coronary CT angiography. *Circ J* 2008; **72:** 671–673.
14. Matsumoto N, Sato Y, Yoda S, Nakano Y, Kunimasa T, Matsuo S, et al. Prognostic value of non-obstructive CT low-dense coronary artery plaques detected by multislice computed tomography. *Circ J* 2007; **71:** 1898–1903.
15. Flohr TG, McCollough CH, Bruder H, Petersilka M, Gruber K, Suss C, et al. First performance evaluation of a dual-source CT (DSCT) system. *Eur Radiol* 2006; **16:** 256–268.
16. Scheffel H, Alkadhi H, Plass A, Vachenauer R, Desbiolles L, Gaemperli O, et al. Accuracy of dual-source CT coronary angiography: First experience in a high pre-test probability population without heart rate control. *Eur Radiol* 2006; **16:** 2739–2747.
17. Achenbach S, Ropers D, Kuettner A, Flohr T, Ohnesorge B, Bruder H, et al. Contrast-enhanced coronary artery visualization by dual-source computed tomography: Initial experience. *Eur J Radiol* 2006; **57:** 331–335.
18. Johnson TR, Nikolaou K, Wintersperger BJ, Leber AW, von Ziegler F, Rist C, et al. Dual-source CT cardiac imaging: Initial experience. *Eur Radiol* 2006; **16:** 1409–1415.
19. Flohr TG, Schoepf UJ, Ohnesorge BM. Chasing the heart new developments for cardiac CT. *J Thorac Imaging* 2007; **22:** 4–16.
20. Leber AW, Johnson T, Becker A, von Ziegler F, Tittus J, Nikolaou K, et al. Diagnostic accuracy of dual-source multi-slice CT-coronary angiography in patients with an intermediate pretest likelihood for coronary artery disease. *Eur Heart J* 2007; **28:** 2354–2360.
21. Johnson TR, Nikolaou K, Busch S, Leber AW, Becker A, Wintersperger BJ, et al. Diagnostic accuracy of dual-source computed tomography in the diagnosis of coronary artery disease. *Invest Radiol* 2007; **42:** 684–691.
22. Weustink AC, Meijboom WB, Mollet NR, Otsuka M, Pugliese F, van Mieghem C, et al. Reliable high-speed coronary computed tomography in symptomatic patients. *J Am Coll Cardiol* 2007; **50:** 786–794.
23. Heuschmid M, Burgstahler C, Reimann A, Brodoefel H, Mysal I, Haeberle E, et al. Usefulness of noninvasive cardiac imaging using dual-source computed tomography in an unselected population with high prevalence of coronary artery disease. *Am J Cardiol* 2007; **100:** 587–592.
24. Oncel D, Oncel G, Tastan A. Effectiveness of dual-source CT coronary angiography for the evaluation of coronary artery disease in patients with atrial fibrillation: Initial experience. *Radiology* 2007; **245:** 703–711.
25. McCollough CH, Primak AN, Saba O, Bruder H, Stierstorfer K, Raupach R, et al. Dose performance of a 64-channel dual-source CT scanner. *Radiology* 2007; **243:** 775–784.
26. Gavaliatsis IP. 'Right posterior' sinus node artery. *Int J Cardiol* 2000; **75:** 301–303.
27. McAlpine WA. Heart and coronary arteries: An anatomical atlas for clinical diagnosis, radiological investigation, and surgical treatment. New York: Springer-Verlag; 1975; 160–178.
28. Nerantzis C, Avgoustakis D. An S-shaped atrial artery supplying the sinus node area: An anatomical study. *Chest* 1980; **78:** 274–278.
29. Rigatelli G, Tranquillo M, Stefano P. Abnormally huge S-shaped sinus node artery: A possible caveat for mitral valve surgery. *Int J Cardiol* 2007; **116:** 401–402.